JSST
Journal of Space Science and Technology

P-ISSN: 2008-4560
E-ISSN: 2423-4516

Journal of Space Science and Technology

Vol. 18, No. 4, pp. 12-21, 2025
https://doi.org/10.22034/jsst.2025.1537
Journal Homepage: https://jsstpub.com

Original Research Paper

A Journey into the Application of the Poincaré Map in the Circular Restricted Three-Body Problem

Ehsan Abbasali[1], Fatemeh Ebrahimian[2], Amirreza Kosari[3*], and Majid Bakhtiari [4]

1-3. School of Aerospace Engineering, College of Interdisciplinary Science and Technologies, University of Tehran, Tehran, Iran
4. School of Advanced Technologies, Iran University of Science and Technologies, Tehran, Iran

ARTICLE INFO

Article History:

Received 18 March 2025
Revised 15 May 2025
Accepted 19 May 2025
Available Online 15 July 2025

Keywords:

Poincaré map
CRTBP
Periodic orbits
Three-body problem

ABSTRACT

This article investigates the identification of periodic orbits and spacecraft attitude behavior in the Circular Restricted Three-Body Problem (CRTBP) using the Poincaré map as an innovative analytical tool. The CRTBP describes the motion of a spacecraft under the gravitational influence of two primary celestial bodies and presents challenges due to the absence of closed-form solutions for both orbital and attitude dynamics. To address this, the study employs the Poincaré map as an efficient numerical method to detect suitable initial conditions for periodic motion, thereby reducing mathematical complexity and improving computational performance. A notable innovation in this work is the integration of spacecraft attitude dynamics into the Poincaré-based analysis. Although the coupling is one-way, meaning attitude states do not influence the periodicity of orbital motion, they do affect the structure of the resulting Poincaré maps. The shape and position of islands on these maps vary with changes in the spacecraft's inertia ratio, which demonstrates the method's sensitivity to attitude behavior and its relevance to real-world applications. The proposed method is benchmarked against two classical techniques: the third-order approximation and Floquet theory-based approaches. Comparative analysis shows that the Poincaré map offers a superior balance of simplicity, computational efficiency, and accuracy. It achieves reliable identification of periodic orbits without requiring high-order models or intricate corrections. Overall, the study provides a novel and practical contribution to space mission design, offering a robust and accessible framework for analyzing trajectory and attitude dynamics in complex gravitational environments such as libration point missions.

* Corresponding Author's E-mail: kosari_a@ut.ac.ir

How to Cite this Article:
E. Abbasali, F. Ebrahimian, A. Kosari, and M. Bakhtiari, "A journey into the application of the poincaré map in the circular restricted three-body problem," *Journal of Space Science and Technology*, Vol. 18, No. 4, pp. 12-21, 2025, https://doi.org/10.22034/jsst.2025.1537.

1. INTRODUCTION

In recent years, the study of multi-body dynamic systems has garnered significant attention, driven by the need for more accurate simulations of spacecraft and satellite motion. These systems offered valuable insights into the natural dynamics of space vehicles, supporting applications such as astronomical observations [1–3], the preparation of human habitats in space, enhanced pointing accuracy for space telescopes, and docking with space stations.

A commonly used approximation for multi-body dynamic systems was the Circular Restricted Three-Body Problem (CRTBP), where a spacecraft moved within the gravitational potential of two celestial bodies. Since the spacecraft's mass was negligible compared to the two primary bodies, their motion remained unaffected by the spacecraft [4]. Consequently, extensive research was conducted on CRTBP: Kunitsyn explored satellite stability around equilibrium points [5], Lega analyzed energy manifolds in CRTBP [6], and Bakhtiari extended the model to study the formation flying of satellite constellations in the elliptic problem [7].

However, the equations of motion governing CRTBP lacked closed-form solutions [4], which necessitated the use of numerical methods. These methods' reliance on initial conditions yielded a vast array of potential trajectories, enabling the identification of countless orbits. Among these, periodic and quasi-periodic structures were particularly valuable for maintaining satellites on well-defined paths and ensuring reliable data transmission. Notably, Halo and Lyapunov orbits formed a prominent class of periodic orbits in CRTBP [8].

Farquhar first introduced the term "Halo orbits" in his doctoral dissertation [9]. He and Kamel later developed an analytical approach using the Lindstedt-Poincaré method to identify quasi-periodic orbits near the Earth-Moon. L_2 Lagrange point [10,11]. In 1979, Breakwell and Brown developed a numerical method to compute strictly periodic orbits around the L_2 point of the Earth-Moon system [12]. Building upon this, Howell proposed a comprehensive numerical method for identifying Halo orbits around the Lagrangian points of the CRTBP in his doctoral dissertation [13]. Further studies included those by Abbasali et al., who extended this algorithm to extract Lyapunov orbits and periodic attitude solutions [14,15]. Moreover, modeling of Halo orbits and stable and unstable manifolds in CRTBP was carried out by Jafari Nadoushan and Pourtakdoust [16]. Kiani et al. investigated optimal transfer trajectory design from Earth-centered orbits to Halo orbits in the Earth-Moon system using a homotopy approach [17]. Increasing the realism of the simulated environment can significantly enhance orbit simulation accuracy. Adding perturbations to the modeled environment proved beneficial in achieving this goal [18]. Orbital analyses in the circular three-body regime, incorporating Earth's oblateness in the Earth-Moon system, were performed by Singh [19]. Srivastava and Kumar studied CRTBP orbits under the influence of Earth's oblateness and solar radiation pressure in the Earth-Sun system [20], utilizing Lagrangian mechanics to derive orbital equations. Non-linear stability of satellites around the Earth-Moon system L_2 point, accounting for Earth's oblateness, was explored by Markellos and Papadakis [21]. Singh extended these studies by considering a spacecraft with variable mass [22]. The effect of Earth's oblateness on hovering satellites operating in low-Earth orbits was investigated by Zhang et al. [23]. Farquhar-Kamel and Howell algorithms utilized a state transition matrix and the residue method to match orbital state parameters for periodic Lyapunov and Halo orbits. This approach involved solving 42 simultaneous differential equations over the orbital period, making it computationally demanding due to the chaotic nature of CRTBP. Researchers often use approximate solutions to generate initial guesses. However, these algorithms frequently failed to refine them accurately. To address this, this study proposes using the Poincaré map to identify initial conditions to obtain periodic responses, offering an efficient method to reduce system dimensionality and analyze critical parameters [24]. We compare the Poincaré map with two other approaches, namely the third-order approximation method and the Floquet theory-based method, focusing on factors such as complexity, efficiency, and precision. The results highlight the advantages of the Poincaré map, which provides a more accurate, efficient, and less complex solution compared to the alternatives.

2. PAPER GEOMETRY OF THE CONSTRAINED THREE-BODY PROBLEM

Two primary celestial bodies with masses m_1 and m_2, where $(m_1 > m_2)$, are assumed to move in circular orbits under mutual gravitational attraction. The spacecraft, with mass m, is considered part of the system, and its equations of motion are determined within the system of interest. The spacecraft's mass is considered negligible compared to the mass of the celestial bodies. In celestial mechanics, this is referred to as the Restricted Three-Body Problem, as the spacecraft's motion does not influence the motion of the primaries (e.g., the spacecraft's mass is negligible relative to the primaries'mass). This study primarily focuses on the motion of the spacecraft within the three-body problem. The resulting model, derived under the two specified conditions, is known as the Circular Restricted Three-Body Problem (CRTBP) and has been widely applied in numerous studies [4]. When the two primary celestial bodies follow specific orbits, a coordinate system can be established that is fixed relative to their motion. The center of mass of this system is chosen as the origin of the required coordinate system, which rotates at a constant angular velocity Ω, equal to the mean motion of the primary planets. This rotating coordinate system is defined by the unit vectors $\mathbf{r}(\hat{x}.\hat{y}.\hat{z})$ Fig. 1, where the $\hat{z}$ component is perpendicular to the orbital plane of the primaries. The primary masses m_1 and m_2 are always positioned along the $\hat{x}$-axis of this coordinate system.

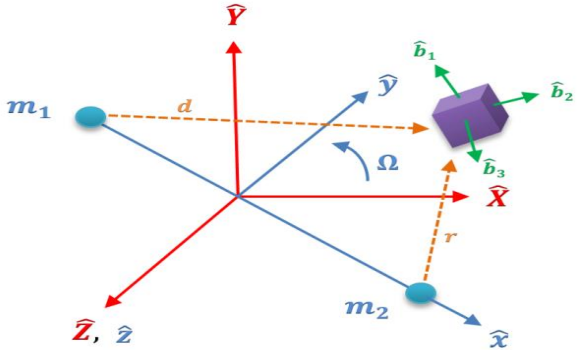

Fig. 1. Geometry of the restricted three-body problem.

Additionally, the inertia frame $\boldsymbol{I}(\hat{X}.\hat{Y}.\hat{Z})$ is defined such that, at the initial time $t = 0$, it is aligned with the rotating coordinate system. In this system, the unit vector $\hat{Z}$ is always aligned with the $\hat{z}$-axis of the rotating coordinate system and remains perpendicular to the orbital plane of the primary planets. To simplify the equations in these coordinates, a non-dimensional form (ndim) is preferred. In this form, the universal gravitational constant G, the angular velocity Ω, and the distance between the two primary planets are normalized to unity. The orbital period of the primary planets is thus 2π, and the mass parameter μ is defined as the ratio of the smaller planet's mass m_2 to the total system mass: $\mu = \frac{m_2}{m_1+m_2}$.

The mass parameter defines the positions of the primary planets such that the larger planet is located at $(-\mu.0.0)$ and the smaller planet at $(1-\mu.0.0)$. The equations of motion in the rotating coordinate system are expressed as:

$$\begin{aligned} \ddot{x} &= 2\dot{y} + U_x^* \\ \ddot{y} &= -2\dot{x} + U_y^* \\ \ddot{z} &= U_z^* \end{aligned} \tag{1}$$

where $U_{(x,y,z)} = -\frac{\mu_1}{d} - \frac{\mu_2}{r} - \frac{1}{2}(x^2+y^2)$ denotes the Pseudo potential function of the CRTBR, and the distances from the bigger and smaller primary are denoted by $d = \sqrt{(x+\mu)^2+y^2+z^2}$ and $r = \sqrt{(x-(1-\mu))^2+y^2+z^2}$; respectively. In addition $\mu_1 = 1-\mu$ represents the gravitational parameter of the larger primary body and $\mu_2 = \mu$ represents the gravitational parameter of the smaller primary body.

3. EQUATIONS OF ROTATIONAL MOTION

The fundamental equations of rotational motion for a rigid body, derived based on Newton's Second Law, are presented in angular velocity form.

The vector of external moments acting on the rigid spacecraft body, expressed in the body-*fixed* frame $\hat{\boldsymbol{b}}$, which is attached to the rigid body and rotates with respect to the inertia frame, is represented as follows:

$$\boldsymbol{M}^B = M_1\hat{b}_1 + M_2\hat{b}_2 + M_3\hat{b}_3 \tag{2}$$

The angular velocity equations, which describe the rotational dynamics of a rigid body about its center of mass, are written as [23,24]:

$$\begin{aligned} I_1\dot{\omega}_1 &= -(I_3-I_2)\omega_2\omega_3 + M_1 \\ I_2\dot{\omega}_2 &= -(I_1-I_3)\omega_1\omega_3 + M_2 \\ I_3\dot{\omega}_3 &= -(I_1-I_1)\omega_1\omega_2 + M_3 \end{aligned} \tag{3}$$

The angular velocity vector is represented by $[\omega_1, \omega_2, \omega_3]$.

In these equations, I_i represents the principal moments of inertia associated with the body axes $\hat{b}_i$ and M_i denotes the components of the external torque vector applied to the satellite's body ($i = 1,2,3$). The time rate of change of the satellite's angular velocities is summarized by the system as follows [25].

$$\begin{aligned}
\dot{\omega}_1 &= \frac{I_3 - I_2}{I_1}\left(\frac{3(1-\mu)}{d^3} g_2 g_3 + \frac{3\mu}{r^3} h_2 h_3 - \omega_2 \omega_3\right) \\
\dot{\omega}_2 &= \frac{I_1 - I_3}{I_2}\left(\frac{3(1-\mu)}{d^3} g_1 g_3 + \frac{3\mu}{r^3} h_1 h_3 - \omega_1 \omega_3\right) \\
\dot{\omega}_3 &= \frac{I_2 - I_1}{I_3}\left(\frac{3(1-\mu)}{d^3} g_1 g_2 + \frac{3\mu}{r^3} h_1 h_2 - \omega_1 \omega_2\right)
\end{aligned} \tag{4}$$

where h_i represents the projection vector of the spacecraft relative to the larger planet m_1, and g_i denotes the projection vector of the spacecraft relative to the smaller planet m_2 in the body-fixed frame. By introducing the direction cosine matrix, the projection vectors h_i and g_i can be expressed as functions of the instantaneous position and orientation of the satellite:

$$\begin{aligned}
\begin{bmatrix} g_1 \\ g_2 \\ g_3 \end{bmatrix} &= \boldsymbol{A}_{\hat{b}.\hat{\imath}} \boldsymbol{A}_{\hat{\imath}.\hat{r}} \frac{\boldsymbol{d}}{d} = \boldsymbol{A}_{\hat{b}.\hat{\imath}} \boldsymbol{A}_{\hat{\imath}.\hat{r}} \frac{1}{d} \begin{bmatrix} x + \mu \\ y \\ z \end{bmatrix} \\
\begin{bmatrix} h_1 \\ h_2 \\ h_3 \end{bmatrix} &= \boldsymbol{A}_{\hat{b}.\hat{\imath}} \boldsymbol{A}_{\hat{\imath}.\hat{r}} \frac{\boldsymbol{r}}{r} = \boldsymbol{A}_{\hat{b}.\hat{\imath}} \boldsymbol{A}_{\hat{\imath}.\hat{r}} \frac{\boldsymbol{1}}{d} \begin{bmatrix} x - 1 + \mu \\ y \\ z \end{bmatrix}
\end{aligned} \tag{5}$$

In Eq. (5), the rotation matrix from inertia to body frame and the rotation matrix from rotating to inertia frame are denoted by $\boldsymbol{A}_{\hat{b}.\hat{\imath}}$ and $\boldsymbol{A}_{\hat{\imath}.\hat{r}}$, respectively.

$$\boldsymbol{A}_{\hat{\imath}.\hat{r}} = \begin{bmatrix} \cos(t) & -\sin(t) & 0 \\ \sin(t) & \cos(t) & 0 \\ 0 & 0 & 1 \end{bmatrix} \tag{6}$$

$$\boldsymbol{A}_{\hat{b}.\hat{\imath}} = \begin{bmatrix} q_1^2 - q_2^2 - q_3^2 + q_4^2 & 2(q_1 q_2 + q_3 q_4) & 2(q_1 q_3 - q_2 q_4) \\ 2(q_1 q_2 - q_3 q_4) & -q_1^2 + q_2^2 - q_3^2 + q_4^2 & 2(q_2 q_3 + q_1 q_4) \\ 2(q_1 q_3 + q_2 q_4) & 2(q_2 q_3 + q_1 q_4) & -q_1^2 - q_2^2 + q_3^2 + q_4^2 \end{bmatrix} \tag{7}$$

where $\boldsymbol{q} = [q_1\ q_2\ q_3\ q_4]$ represents quaternion vectors, and Eq. (8) is used to propagate quaternions in time.

$$\begin{aligned}
\dot{q}_1 &= \frac{1}{2}(\omega_3 q_2 - \omega_2 q_3 + \omega_1 q_4) \\
\dot{q}_2 &= \frac{1}{2}(-\omega_3 q_1 + \omega_1 q_3 + \omega_2 q_4) \\
\dot{q}_3 &= \frac{1}{2}(\omega_2 q_1 - \omega_1 q_2 + \omega_3 q_4) \\
\dot{q}_3 &= \frac{1}{2}(-\omega_1 q_1 - \omega_2 q_2 - \omega_3 q_3)
\end{aligned} \tag{8}$$

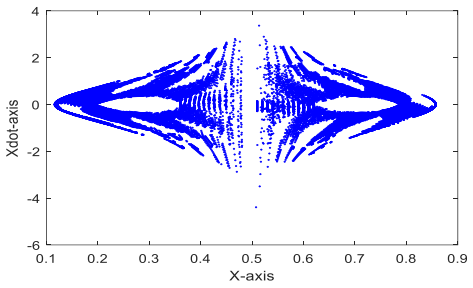

Fig. 2. Simulation of the Poincaré map to obtain initial conditions of the periodic orbits orbits regarding $x_{0_p} = 0.8$ and $\dot{x}_{0_p} = 0.4$.

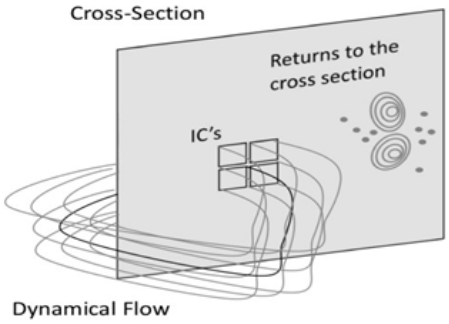

Fig. 3. Schematic of the Poincaré map [20].

4. EQUATIONS SOLVING METHODS

The system of Eqs. (1,4,8) represents the governing orbit and attitude dynamics of spacecraft motion within the Circular Restricted Three-Body Problem (CRTBP). As these equations lack closed-form solutions, their resolution necessitates the application of numerical methods. Given the sensitivity of numerical solutions to initial conditions, obtaining periodic solutions requires precisely defined and accurate initial conditions for the system's state variables. The scarcity of periodic solutions further highlights the critical need for high precision in specifying these initial conditions.

In prior research, suitable initial conditions for identifying periodic solutions were derived by approximately solving the equations of motion in the CRTBP. This was achieved using a residue method in conjunction with an orbital correction algorithm. However, this methodology involved complex and computationally intensive mathematical procedures. Moreover, determining each periodic solution necessitated the provision of a carefully selected initial guess as an input for the orbital correction algorithm. Therefore, this paper

proposes a Poincaré map to obtain the appropriate initial conditions. For comparison purposes, the performance of the Poincaré map will be qualitatively compared with the methods used in previous studies in the results section.

4.1 Poincaré Map

In this article, the Poincaré map is proposed as a method to identify the initial conditions for periodic orbit-attitude responses within the Circular Restricted Three-Body Problem CRTBP. The Poincaré map serves as a powerful tool for capturing the dynamical structures of an n-dimensional system, such as periodic or quasi-periodic trajectories, described by the system of equations $\dot{\boldsymbol{x}} = \boldsymbol{f}(x)$ .This method is grounded in analyzing the dynamical flow of the system.

To apply this technique, an $n-1$-dimensional cross-section perpendicular to the dynamical flow was defined, and a set of initial guesses was distributed on this section Fig. 2 Using the system's governing equations, these initial guesses are propagated iteratively, and each intersection of the dynamical flow with the cross-section is recorded and visualized. It is important to note that the chosen cross-section can represent any combination of the system's state variables.

The intersections of the dynamical flow with the defined cross-section are depicted based on the state variables. When two state variables are considered, each intersection is represented as a single point on the two-dimensional cross-section. Although two parameters may not provide a complete description of the system's state, they are often sufficient to reveal the dynamical structures of interest.

Specifically, periodic and quasi-periodic structures manifest as two-dimensional patterns aligned along closed curves on the Poincaré map's cross-section. These closed curves do not exist independently but instead cluster into islands. The centers and boundaries of these islands are regarded as indicative of periodic solutions. To better illustrate the implementation of this method, an example is provided.

For periodic orbits, the parameters of interest are the position x and velocity v_x, which have been empirically determined [18]. Similarly, for rotational dynamics, the corresponding quaternion and angular velocity components, such as q_2 and ω_2, are chosen to define the mapping plane [18].

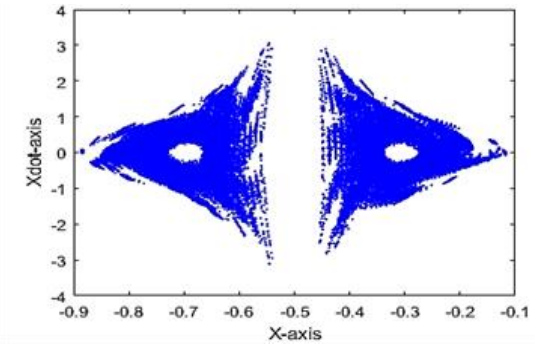

Fig. 4. Simulation of the Poincaré map to obtain initial conditions of the periodic orbits regarding $x_{0_p} = -0.5$ and $\dot{x}_{0_p} = -0.4$.

Initially, a plane consisting of the specified parameters was defined as the cross-section. Arbitrary initial guesses for these parameters are distributed across the plane. Next, various solutions, such as successive iterations for a chosen period, are computed using the dynamical flow (i.e., propagation of the system's governing equations). Each time the dynamical flow intersects the cross-section, the corresponding values of the parameters of interest are recorded and represented as a single point on the map.

In subsequent iterations, one of the parameters is fixed to the same value used in the initial guess for the first solution. The initial guesses for the remaining parameters are updated to the values recorded from the previous solution on the cross-section. The period is kept constant across all solutions.

The islands formed on the Poincaré map (regions of higher point density) and their boundaries identify the appropriate initial conditions for the orbital parameters to achieve periodic solutions. Furthermore, if these islands appear, the selected periodicity will correspond to the period of the identified periodic orbit. We want to note that changes in the initial conditions of Lyapunov orbits directly influence the simulation of the Poincaré map, as described by Equation (8). Specifically, such changes modify the Jacobi constant C, which plays a fundamental role in the dynamics of the system by defining the zero-velocity surfaces and constraining the motion of the particle:

$$\dot{y} = \sqrt{2U(x,y,z) - C} \tag{8}$$

Although the Jacobi constant remains fixed along a given periodic orbit, it varies from one orbit

to another as the initial conditions change. Consequently, variations in C can alter the structure of the Poincaré map and affect the existence, location, and stability of periodic orbits.

5. RESULTS

5.1 Orbital Analysis

The primary objective of this paper is to elucidate the application of the Poincaré map within the context of the Circular Restricted Three-Body Problem (CRTBP). To illustrate this concept effectively, we will focus on the Cislunar system, specifically the Earth-Moon system, as our case study. The constants relevant to this system are detailed in Tab. 1.

Table 1. Constants of the cislunar system.

$\mu_{Cislunar}$	$R_{Earth}\ (km)$	$R_{Moon}\ (km)$
0.01215	6378	1734.4

In the initial analysis, the periodic orbit initial conditions are determined using the Poincaré map. For this purpose, we focus on establishing a family of periodic orbits in the vicinity of the L_1 Lagrangian point. The L_1 Lagrangian point is located approximately at $x_{L_1} = 0.8\ (ndim)$ and $y_{L_1} = 0\ (ndim)$. Therefore, we assume an initial guess for our simulation of the Poincaré map with $x_{0_p} = 0.8$. Additionally, we set the initial velocity in the x-direction, $\dot{x}_{0_p} = 0.4$. In this simulation, the Runge–Kutta–Fehlberg method (RKF45) implemented in MATLAB was used as the numerical solver, with a fixed step size of 0.001 seconds. Note that there is no convergence criterion; the process continues until the iterative solution of Eq. (1) is completed for each chosen set of initial conditions for x and $\dot{x}$. The more initial guesses are considered, the higher the accuracy of the resulting map and the greater the chance of revealing additional islands.

The results of this simulation are presented in Fig. 4. By analyzing these results, we aim to gain insights into the structure of the phase space around the L_1 point and to understand the potential for mission design strategies that leverage these periodic orbits.

To validate the results, we have plotted several of the identified periodic orbits in Fig. 5, using initial conditions extracted from the Poincaré map in Fig. 3. Each point on the boundary of the island can be considered a suitable initial condition. A summary of some of the initial conditions used in Fig. 5 is presented in Tab. 2, where the orbital period is denoted by T.

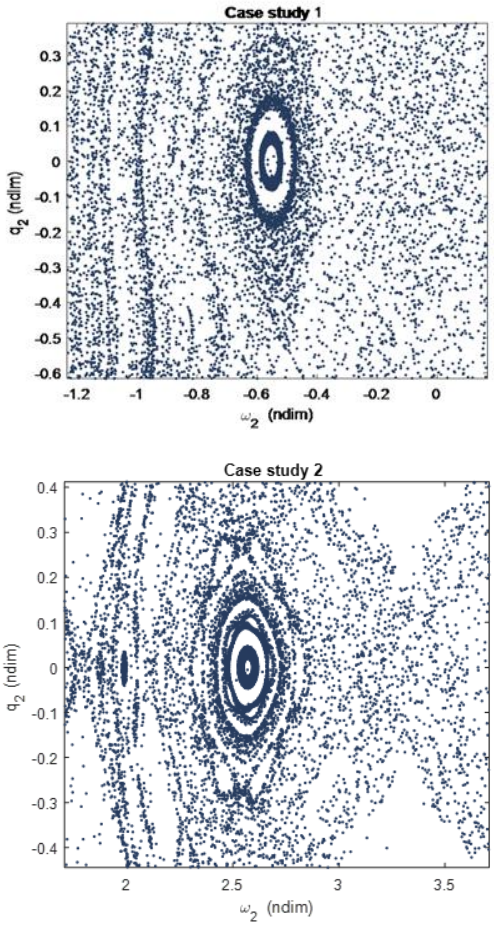

Fig. 5. Poincaré map simulation for the spacecraft attitude dynamics considering $K_1 = 0.75, K_2 = -0.75$ and $K_3 = 0$.

Table 2. Initial conditions of the periodic orbits in Fig. 3.

Orbit number	$x_0(ndim)$	$\dot{x}_0(ndim)$	$T\ (ndim)$
Orbit 1	0.983	0.437	3.56
Orbit 2	0.987	0.439	3.74
Orbit 3	0.989	0.441	3.80
Orbit 4	0.995	0.449	3.82
Orbit 5	1.066	0.452	3.87

5.2 Attitude Analysis

For the second analysis, the application of the Poincaré map was used to identify the initial conditions of the attitude states required to achieve periodic behavior in the attitude dynamics. As in the

previous simulation of the Poincaré map for the periodic responses of the orbital motion, the Runge–Kutta–Fehlberg method (RKF45) implemented in MATLAB was used as the numerical solver, with a fixed step size of 0.001 seconds. This same consideration was also applied to simulate the Poincaré map for the periodic responses of the attitude behavior. As mentioned, the more initial guesses that are considered, the higher the accuracy of the resulting map and the greater the likelihood of revealing additional islands.

Since the orbital states influence the attitude states (as shown in Eqs. (3, 4), a periodic orbit, specified in Table 2, is first selected. For this analysis, Orbit 1 is selected. We assumed the initial attitude state values from Table 3 to simulate the Poincaré map and identify appropriate conditions for periodic response. Additionally, the following inertia ratios are considered: $K_1 = 0.75, K_2 = -0.75$ and $K_3 = 0$.

Table 3. Initial guess of the attitude states to simulate the Poincaré map considering orbit 1.

	q_1	q_2	q_3	ω_1	ω_2	ω_3
Case study 1	0.7	0	0.7	1	0	-0.5
Case study 2	1	0	0	0	-2	0

As mentioned, the Poincaré map for attitude states is simulated for corresponding parameters like $q_2 - \omega_2$. The results of the Poincaré map simulation are illustrated in Fig. 6 for Case Studies 1 and 2.

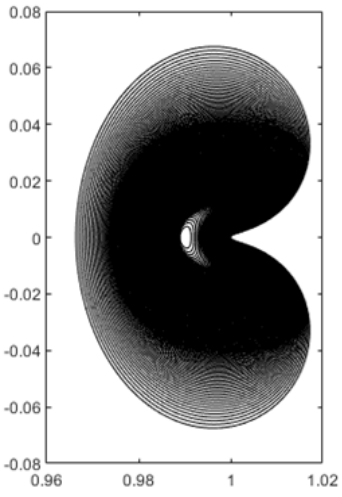

Fig. 6. Some of the periodic orbits of the Cislunar system.

As previously discussed, the points located at the boundaries of the islands can be selected as appropriate initial conditions for the attitude states. The research conducted in this study indicates that decreasing the inertia ratio values reduces the likelihood of identifying periodic solutions.

For instance, if the same initial guess provided in Table 3 was used, but the inertia ratio values were changed to : $K_1 = 0.55, K_2 = -0.55$ and $K_3 = 0$, the Poincaré map simulation results, originally shown in Fig. 6, will change as illustrated in Fig. 7.

A comparison between Fig. 6 and Fig. 7 shows that decreasing the inertia ratio, while keeping the initial guesses for the orbital and attitude states unchanged, results in an increase in the number of islands appearing in the Poincaré maps of the attitude states. Consequently, this increases the likelihood of obtaining periodic responses.

In this study, the Poincaré map method was used to identify periodic solutions for both orbital and attitude dynamics. To evaluate its effectiveness, it is compared qualitatively with two alternative approaches. The first is the third-order approximation method, which, despite its theoretical foundation, is highly complex mathematically, time-consuming, and lacks the precision needed for reliable identification of periodic solutions. The second is the Floquet theory-based method, which is more accurate but suffers from significant mathematical complexity and requires an additional differential correction algorithm, adding to its computational demands. In contrast, the Poincaré map method offers a more efficient and straightforward solution.

It eliminates the need for complex approximations or correction algorithms while maintaining high accuracy and computational efficiency. This makes it a practical and user-friendly tool for analyzing periodic behavior in dynamic systems. The qualitative comparison is summarized in Table 4:

Table 4. Qualitative comparison of the Poincaré map method with third-order approximation and Floquet theory-based methods.

Criteria	Poincaré map	Third-order approximation	Floquet theory-based
Mathematical Complexity	Low	High	High
Computational Efficiency	High	Low	Moderate
Accuracy	High	Low	High
Ease of Implementation	High	Low	Moderate

It is clarified that the Floquet theory-based method focuses primarily on identifying periodic attitude motions through stability analysis of the state transition matrix of the attitude dynamics. The state transition matrix is computed for various initial guesses and inertia ratios over specified time intervals, and a stability assessment is then performed using the corresponding eigenvalues and eigenvectors. A mathematically intensive procedure, as detailed in [15], is applied to each eigenvalue–eigenvector pair to generate a 3D contour map involving inertia ratios, eigenvalues, and a stability index. From this contour, the initial conditions corresponding to periodic attitude responses are identified. This method is not applicable to the identification of periodic orbital motion and presents significant mathematical complexity, which may be considered a drawback compared to the proposed Poincaré map-based method.

Likewise, the third-order approximation method, as described in [15,20,22], is limited to identifying initial conditions for periodic orbital motion and has not been extended to attitude motion identification in the restricted three-body problem. This method also involves a complex solution procedure and typically yields only one initial condition per execution. In contrast, the proposed Poincaré map-based approach enables the identification of both periodic orbital and attitude initial conditions, offers a simpler implementation process, and can identify multiple candidate conditions in a single execution.

Finally, it must be noted that the Poincaré map has certain limitations that should be acknowledged to provide readers with a clearer understanding of its applicability. For this reason, two of its main limitations are discussed below.

The first limitation concerns the method's sensitivity to the initial conditions used in the simulations. For some initial conditions, no islands may appear in the generated maps, meaning that no periodic response conditions can be identified. The selection of suitable initial conditions that result in the appearance of islands is entirely empirical and lacks a precise solution. To illustrate this, Fig. 7 shows the Poincaré map plotted for the same initial orbital and attitude state vectors, once with an inertia ratio of 0.05 and once with 0.4.

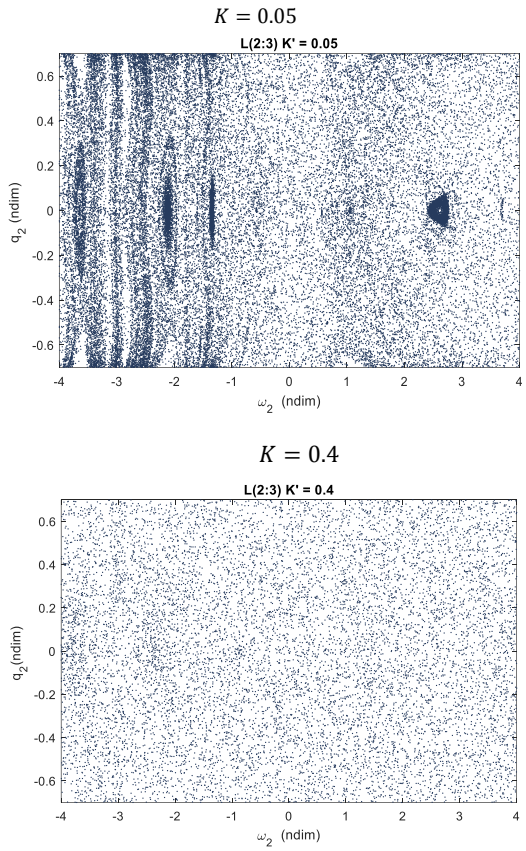

Fig. 7. Poincaré maps for two inertia ratios showing the method's sensitivity to initial conditions.

As shown, for the inertia ratio of 0.4, no islands appear, and hence no periodic response can be identified. It should be noted that the inertia ratio in this analysis is determined through trial and error, and after testing several values, the appropriate inertia ratio of 0.05, for which islands appear, was identified experimentally. There is no exact method to determine in advance which value will lead to the appearance of islands. Therefore, this approach is highly sensitive to initial conditions and lacks a systematic method for their selection.

The second limitation relates to the dimensionality of the problem. In the current case, the problem is such that by selecting two state parameters and generating a 2D map based on them, the initial conditions of periodic responses can be identified. However, it should be considered that in higher-dimensional problems, it may be necessary to plot the map using, for instance, four state parameters, which is practically infeasible. As a result, the use of the Poincaré map in such high-dimensional cases may not be viable.

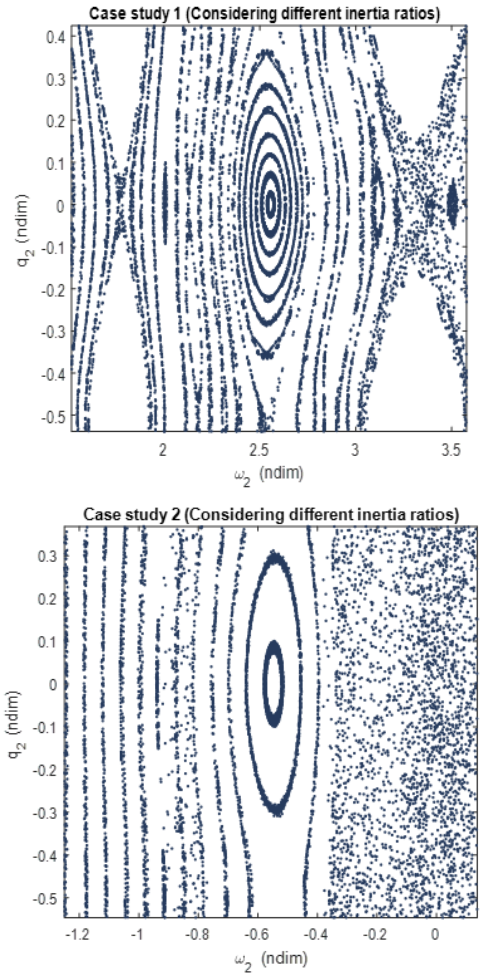

Fig. 8. Poincaré map simulation for the spacecraft attitude dynamics considering $K_1 = 0.55, K_2 = -0.55$ and $K_3 = 0$.

6. CONCLUSION

This article presents an innovative approach to identifying periodic orbits and attitude behavior of spacecraft in the Circular Restricted Three-Body Problem (CRTBP) using the Poincaré map. The governing equations of orbital motion and attitude dynamics were utilized; however, due to the absence of closed-form solutions, numerical methods became essential. Depending on the initial state parameters, the system exhibited either periodic or non-periodic behavior. To address this challenge, the Poincaré map was introduced as a novel and effective innovation that facilitates the identification of appropriate initial conditions to yield periodic responses, thereby significantly reducing the mathematical complexity of the analysis.

One innovative finding of this study is that, for identical initial conditions but varying spacecraft inertia ratios, the location of islands on the Poincaré map changes. This demonstrates that the inertia ratio is a critical parameter, with smaller values increasing the likelihood of periodic solutions. Furthermore, the Poincaré map method was evaluated against two established alternatives—the third-order approximation and the Floquet theory-based method—in terms of mathematical complexity, computational efficiency, and accuracy. The comparison revealed that the Poincaré map represents an innovative and superior solution, offering simplicity, high accuracy, and efficiency without requiring complex corrections or approximations.

CONFLICTS OF INTEREST

The authors declare that they have no conflict of interest.

REFERENCES

[1] J. P. Gardner *et al.*, "The James webb space telescope," *Space Science Reviews*, vol. 123, no. 4, pp. 485-606, 2006, https://doi.org/10.1007/s11214-006-8315-7.

[2] P. Kalas, "In the spirit of Bernard Lyot: The direct detection of planets and circumstellar disks in the 21st century," in *Conference in the Spirit of Bernard Lyot*, University of California, Berkeley, CA, USA, 2007.

[3] M. Machula and G. Sandhoo, "Rendezvous and docking for space exploration," in *1st Space Exploration Conference: Continuing the Voyage of Discovery*, Orlando, Florida, 2005, Paper 2716, https://doi.org/10.2514/6.2005-2716.

[4] H. D. Curtis, *Orbital Mechanics for Engineering Students*, 3rd ed. Netherlands, Elsevier Science, 2013.

[5] A. L. Kunitsyn, "The stability of triangular libration points in the photogravitational three-body problem," *Journal of Applied Mathematics and Mechanics*, vol. 64, no. 5, pp. 757-763, 2000, https://doi.org/10.1016/S0021-8928(00)00105-2.

[6] E. Lega and M. Guzzo, "Three-dimensional representations of the tube manifolds of the planar restricted three-body problem," *Physica D: Non-linear Phenomena*, vol. 325, pp. 41-52, 2016, https://doi.org/10.1016/j.physd.2016.02.012.

[7] M. Bakhtiari, K. Daneshjou, and E. Abbasali, "A new approach to derive a formation flying model in the presence of a perturbing body in inclined elliptical

orbit: Relative hovering analysis," *Astrophysics and Space Science*, vol. 362, 2017, Art. no. 36, https://doi.org/10.1007/s10509-016-2968-9.

[8] B. Wong, R. Patil, and A. Misra, "Attitude dynamics of rigid bodies in the vicinity of the Lagrangian points," *Journal of Guidance, Control, and Dynamics*, vol. 31, no. 1, pp. 252-256, 2008, https://doi.org/10.2514/1.28844.

[9] R. W. Farquhar, "The control and use of libration-point satellites," Ph.D. dissertation, Department of Aeronautics and Astronautics, Stanford University, Stanford, CA, USA. 1969.

[10] R. W. Farquhar and A. A. Kamel, "Quasi-periodic orbits about the translunar libration point," *Celestial Mechanics*, vol. 7, no. 4, pp. 458-473, 1973, https://doi.org/10.1007/BF01227511.

[11] A. Casal and M. Freedman, "A Poincaré-Lindstedt approach to bifurcation problems for differential-delay equations," *IEEE Transactions on Automatic Control*, vol. 25, no. 5, pp. 967-973, 1980, https://doi.org/10.1109/TAC.1980.1102450.

[12] J. V. Breakwell and J. V. Brown, "The 'Halo' family of 3-dimensional periodic orbits in the Earth-Moon restricted 3-body problem," *Celestial mechanics*, vol. 20, no. 4, pp. 389-404, 1979, https://doi.org/10.1007/BF01230405.

[13] K. C. Howell, "Three-dimensional, periodic, 'Halo' orbits," *Celestial mechanics*, vol. 32, no. 1, pp. 53-71, 1984, https://doi.org/10.1007/BF01358403.

[14] E. Abbasali, A. R. Kosari, and M. Bakhteiari, "Restricted three-body problem considering the perturbations of both oblate massive primaries," *Journal of Aerospace Science and Technology*, vol. 13, no. 2, pp. 27-35, 2020, https://doi.org/10.22034/jast.2021.128013.

[15] E. Abbasali, A. R. Kosari, and M. Bakhtiari, "Effects of oblateness of the primaries on natural periodic orbit-attitude behaviour of satellites in three body problem," *Advances in Space Research*, vol. 68, no. 11, pp. 4379-4397, 2021, https://doi.org/10.1016/j.asr.2021.08.026.

[16] M. Jafari Nadoushan and S. H. Pourtakdoust, "Modeling Halo orbits and the associated manifolds in the restricted three body problem," *Journal of Space Science and Technology*, vol. 3, no. 1, pp. 75-80, 2010.

[17] G. Heydari, M. Kiani, S. H. Pourtakdost, and M. Sayanjali, "Optimal placement of Piezoelectric sensor/actuator patches on sandwich panels considering debonding effects," *Journal of Space Science and Technology*, vol. 13, no. 2, pp. 25-38, 2020, https://doi.org/10.30699/jsst.2020.1195.

[18] Y. J. Qian, X. D. Yang, G. Q. Zhai, and W. Zhang, "Planar periodic orbits' construction around libration points with invariant manifold technique," *Proceedings of the Institution of Mechanical Engineers, Part G: Journal of Aerospace Engineering*, vol. 233, no. 2, pp. 498-509, 2019, https://doi.org/10.1177/0954410017736544.

[19] J. Singh and V. U. Cyril-Okeme, "Perturbed robe's circular restricted three-body problem under an oblate primary," *New Astronomy*, vol. 34, pp. 114-119, 2015, https://doi.org/10.1016/j.newast.2014.06.006.

[20] V. K. Srivastava, J. Kumar, and B. S. Kushvah, "Regularization of circular restricted three-body problem accounting radiation pressure and oblateness," *Astrophysics and Space Science*, vol. 362, 2017, Art. no. 49, https://doi.org/10.1007/s10509-017-3021-3.

[21] V. V. Markellos, K. E. Papadakis, and E. A. Perdios, "Non-linear stability zones around triangular equilibria in the plane circular restricted three-body problem with oblateness," *Astrophysics and Space Science*, vol. 245, pp. 157-164, 1996, https://doi.org/10.1007/BF00637811.

[22] J. Singh, "Non-linear stability in the restricted three-body problem with oblate and variable mass," *Astrophysics and Space Science*, vol. 333, pp. 61-69, 2011, https://doi.org/10.1007/s10509-010-0572-y.

[23] L. Zhang and P. Ge, "High precision dynamic model and control considering J2 perturbation for spacecraft hovering in low orbit," *Advances in Space* Research, vol. 67, no. 7, pp. 2185-2198, 2021, https://doi.org/10.1016/j.asr.2021.01.015.

[24] P. Channell Jr, G. Cymbalyuk, and A. Shilnikov, "Applications of the Poincaré mapping technique to analysis of neuronal dynamics," *Neurocomputing*, vol. 70, no. 10-12, pp. 2107-2111, 2007, https://doi.org/10.1016/j.neucom.2006.10.091.

[25] J. A. Arredondo, J. Guo, C. Stoica, and C. Tamayo, "On the restricted three body problem with oblate primaries," *Astrophysics and Space Science*, vol. 341, pp. 315-322, 2012, https://doi.org/10.1007/s10509-012-1085-7.